Conformational properties of prion strains can be transmitted to recombinant prion protein fibrils in real-time quaking-induced conversion

Kazunori Sano[1], Ryuichiro Atarashi[1,2#], Daisuke Ishibashi[1], Takehiro Nakagaki[1], Katsuya Satoh[1], Noriyuki Nishida[1]

[1]Department of Molecular Microbiology and Immunology, Nagasaki University Graduate School of Biomedical Sciences, Nagasaki, Japan

[2]Research Centre for Genomic Instability and Carcinogenesis, Nagasaki University, Nagasaki, Japan.

[#]Corresponding author: Ryuichiro Atarashi

Department of Molecular Microbiology and Immunology, Nagasaki University Graduate School of Biomedical Sciences, 1-12-4 Sakamoto, Nagasaki 852-8523, Japan.

Tel.: +81-95-819-7059, Fax: +81-95-819-7060, E-mail: atarashi@nagasaki-u.ac.jp

17

18 Running title: Transmission of prion strain-specific properties

19

20 Word counts: 249 for the abstract; 145 for the importance

21

Abstract

The phenomenon of prion strains with distinct biological characteristics has been hypothesized to be involved in the structural diversity of abnormal prion protein (PrP^{Sc}). However, the molecular basis of the transmission of strain properties remains poorly understood. Real-time quaking-induced conversion (RT-QUIC) is a cell-free system that uses *E. coli*-derived recombinant PrP (rPrP) for the sensitive detection of PrP^{Sc}. To investigate whether properties of various prion strains can be transmitted to amyloid fibrils consisting of rPrP (rPrP-fibrils) using RT-QUIC, we examined the secondary structure, conformational stability and infectivity of rPrP-fibrils seeded with PrP^{Sc} derived from either the Chandler or 22L strain. In the first round of the reaction there were differences in the secondary structures, especially in bands attributed to β-sheets, as determined by infrared spectroscopy, and conformational stability between Chandler-seeded (1^{st}-rPrP-fib^{Ch}) and 22L-seeded rPrP-fibrils (1^{st}-rPrP-fib^{22L}). Of note, specific identifying characteristics of the two rPrP-fibril-types seen in the β-sheets resembled those of the original PrP^{Sc}. Furthermore, the conformational stability of 1^{st}-rPrP-fib^{Ch} was significantly higher than that of 1^{st}-rPrP-fib^{22L}, as with Chandler- and

22L-PrP^{Sc}. The survival periods in mice inoculated with 1^{st}-rPrP-fib^{Ch} or 1^{st}-rPrP-fib^{22L} were significantly shorter than those of the mice inoculated with mock 1^{st}-QUIC mixtures. In contrast, these biochemical characteristics were no longer evident in subsequent rounds, suggesting that nonspecific uninfected rPrP-fibrils became predominant probably because of their rapid growth rate. Together, these findings show that at least some strain-specific conformational properties can be transmitted to rPrP-fibrils and unknown cofactors or environmental conditions may be required for further conservation.

Importance

The phenomenon of prion strains with distinct biological characteristics is assumed to result from the conformational variations in the abnormal prion protein (PrP^{Sc}). However, important questions remain about the mechanistic relationship between the conformational differences and the strain diversity, including how to transmit strain-specific conformations. In this study, we investigated whether properties of diverse prion strains can be transmitted to amyloid fibrils consisting of *E. coli*-derived recombinant PrP (rPrP) generated in the real-time quaking-induced conversion

(RT-QUIC), a recently-developed *in vitro* PrP^{Sc} formation method. We demonstrate that at least some of the strain-specific conformational properties can be transmitted to rPrP-fibrils in the first round of RT-QUIC by examining the secondary structure, conformational stability and infectivity of rPrP-fibrils seeded with PrP^{Sc} derived from either the Chandler or 22L prion strain. We believe that these findings will advance our understanding of the conformational basis underlying prion strain diversity.

Introduction

Prion diseases, or transmissible spongiform encephalopathies (TSE), are infectious and fatal neurodegenerative disorders characterized by progressive spongiform changes and the accumulation of abnormal prion protein (PrP^{Sc}) in the central nervous system. Although the pathogenic mechanisms have not been fully elucidated, prion disease is thought to occur through autocatalytic conversion of normal prion protein (PrP^{C}) to PrP^{Sc} (1, 2), known as the protein-only hypothesis. Some biophysical properties are known to differ between PrP^{C} and PrP^{Sc}. PrP^{C} is monomeric, detergent-soluble and protease-sensitive, while PrP^{Sc} is polymeric, detergent-insoluble and partially

protease-resistant (3). These differences are most likely due to the different conformations of the two isoforms. PrP^{C} is largely α-helical, whereas PrP^{Sc} is substantially enriched in β-sheets (4, 5), frequently resulting in amyloid fibril formation.

The existence of diverse prion strains in mammalian species manifesting in phenotypic differences is well known. The strain-specific characteristics are usually maintained upon serial passage in the same species, and may be explained by conformational variations in the PrP^{Sc}. Indeed, strain-dependent differences in β-sheet-rich structures of PrP^{Sc} have been demonstrated by infrared spectroscopy (6-9). In addition, the conformational stability of PrP^{Sc} differed among prion strains, as demonstrated by guanidine hydrochloride (GdnHCl) denaturation assay followed by protease digestion (10, 11). However, the mechanistic relationship between PrP^{Sc} conformational differences and the molecular basis of prion strains remains poorly understood.

Various *in vitro* PrP^{Sc} formation methods have been developed to elucidate the pathogenesis of the prion diseases. One of these methods, protein misfolding cyclic amplification (PMCA), enabled an exponential amplification of PrP^{Sc} *in vitro* by

86 sonication-induced fragmentation of large PrP^{Sc} polymers into smaller units (12). The
87 amplified PrP^{Sc} was accompanied by an increase in infectivity using normal brain
88 homogenate (BH) as a source of PrP^{C} substrates (BH-PMCA) (13). Furthermore, PrP^{Sc}
89 generated by BH-PMCA from five different mouse prion strains retained the
90 strain-specific properties (14). In addition, prion infectivity could be propagated when
91 purified brain-derived PrP^{C} or baculovirus-derived PrP^{C} was used as substrates in the
92 presence of certain cofactors such as nucleic acids and BH from PrP-deficient mice
93 (15-17). These results provide strong evidence to support the protein-only hypothesis, but
94 the structural basis of prion pathogenesis, including the tertiary structure of PrP^{Sc}, has not
95 been fully clarified.

96 On the other hand, the use of *E. coli*-derived purified recombinant PrP (rPrP)
97 offers an advantage over conformational analyses, which generally require a high purity
98 and a large quantity of the target protein. Spontaneously-polymerized amyloid fibrils of
99 rPrP have been reported to induce the accumulation of PrP^{Sc} in the brains of
100 PrP-overexpressing transgenic (Tg) mice (18-20) and some wild-type hamsters (21),
101 however the incubation periods spanned no less than several hundred days and none of

the wild-type hamsters developed any neurological signs at first passage, indicating that the level of infectivity generated in these studies is very low. More recently, wild-type mice developed clinical disease typical of TSE around 130 days after injection of proteinase K-resistant rPrP fibrils (rPrP-fibrils) generated by unseeded-PMCA in the presence of 1-palmitoyl-2-oleoylphosphatidylglycerol (POPG), a synthetic lipid molecule, and total liver RNA (22). Although these results were reproduced by the same group (23), others have reported that rPrP-fibrils generated by the same method were unable to induce either neuropathological changes or the accumulation of PrP^{Sc} (24). Thus, the role of POPG and RNA in the de novo generation of infectious rPrP-fibrils remains controversial.

Meanwhile, two different seeded-PMCA reaction studies using rPrP (rPrP-PMCA) as a substrate have demonstrated the propagation of moderate levels of prion infectivity. One study showed that hamster rPrP can be converted to rPrP-fibrils capable of inducing TSE in the presence of SDS, a synthetic anionic detergent, but there were great variations in the attack rate and the incubation period, which ranged from 119 to 401 days (25). Another study revealed that phosphatidylethanolamine (PE), a

118 phospholipid found in biological membranes, enhances conversion of mouse rPrP into
119 rPrP-fibrils capable of inducing TSE after around 400 days of incubation periods with a
120 100% attack rate (26, 27). Of note, three different strains used as a seed were converted
121 into a single strain with unique strain properties during the serial rPrP-PMCA
122 experiments (27). These studies suggest that a certain amphipathic molecule such as PE is
123 a required cofactor for the propagation of prion infectivity *in vitro*, but not for the
124 transmission of strain-specific properties.

125 The recently developed "real-time quaking-induced conversion" (RT-QUIC) is
126 a sensitive prion detection method (28, 29), in which intermittent shaking enhances the
127 conversion of soluble rPrP into amyloid fibrils in the presence of PrP^{Sc}. The aim of the
128 present research was to investigate whether properties of diverse prion strains can be
129 transmitted to rPrP-fibrils generated in the RT-QUIC. We produced proteinase K-resistant
130 rPrP-fibrils seeded with minute quantities of mouse-adapted scrapie (Chandler or 22L
131 strain) PrP^{Sc} and investigated the secondary structure, conformational stability and
132 infectivity.

133

MATERIALS AND METHODS

Recombinant mouse PrP expression and purification

Recombinant PrP (rPrP) equivalent to residues 23-231 of the mouse PrP sequence was expressed, refolded into a soluble form, and purified essentially as previously described (30). The concentration of rPrP was determined by measuring the absorbance at 280 nm. The purity of the final protein preparations was ≥ 99 %, as estimated by SDS-PAGE, immunoblotting and liquid chromatography-mass spectrometry (data not shown). After purification, aliquots of the proteins were stored at -80 ^{o}C in 10 mM phosphate buffer, pH6.8 or distilled water.

Preparation of brain homogenates

Brain tissues were homogenized at 10% (w/v) in ice-cold PBS supplemented with a protease inhibitor mixture (Roche) using a multi-bead shocker (Yasui Kikai, Osaka, Japan). After centrifugation at 2,000 g for 2 min, supernatants were collected and frozen at -80 ^{o}C until use. Total protein concentrations were determined by the BCA protein

assay (Pierce). The PrP^{Sc} concentrations in the brain homogenates were estimated by dot-blot analysis using a reference standard of rPrP, as previously described (31).

RT-QUIC experiments

We prepared reaction mixtures in a 96-well, optical, black bottom plate (Nunc 265301) to a final total volume of 100 µl. To avoid contamination, we prepared non-infectious materials inside a biological safety cabinet in a prion-free laboratory and used aerosol-resistant tips. The final concentrations of reaction buffer components were 300 mM NaCl, 50 mM HEPES pH 7.5, and 10 µM Thioflavin T (ThT). The concentration of rPrP was 50 or 100 µg/ml, and only freshly-thawed rPrP was used. Brain homogenate was diluted with reaction buffer prior to the reactions. The 96-well plate was covered with sealing tape (Nunc 236366) and incubated at 40 ^{o}C in a plate reader (Infinite M200 fluorescence plate reader, TECAN) with intermittent shaking, consisting of 30 s of circular shaking at the highest speed and no shaking for 30 s, with a 2 min pause to measure the fluorescence. The kinetics of amyloid formation was monitored by the bottom reading of the fluorescence intensity every 10 min using 440-nm excitation and

485-nm emission wavelength of monochromators.

RT-QUIC products analysis

For detection of protease-resistant rPrP, 10 μl of the QUIC samples (1 μg of rPrP) was diluted with 40μl of buffer (300 mM NaCl, 50 mM HEPES pH 7.5) and digested with 10 μg/ml of proteinase K (PK) at 37 ºC for 1 h. After adding Pefabloc (Roche) at a final concentration of 4 mM and 20 μg of thyroglobulin, the proteins were precipitated with 4 volumes of methanol. The samples were heated in sample buffer (2% SDS, 5% β-mercaptoethanol, 5% sucrose, 0.005% bromophenol blue and 62.5 mM Tris-HCl; pH 6.8) at 95 ºC for 5 min, and then loaded onto 10% BisTris NuPAGE gels (Invitrogen). Proteins were transferred onto polyvinylidene difluoride membranes (Millipore, Billerica, MA, USA). The membranes were probed with polyclonal anti-PrP antibody R20 (epitope located at mouse PrP amino acids 218-231) or ICSM35 (D-Gen, London, UK).

Transmission electron microscopy

Negative staining was done on carbon supporting film grids, which were glow-discharged

before staining. The 10 μl samples were adsorbed to the grids for 3 min, then the residual solution was absorbed by filter paper. The grids were stained with 20 μl of fleshly filtered stain (2% uranyl acetate). Once dry, the samples were viewed in a transmission electron microscope (JEM-1200EX, JEOL, Japan).

Fourier transform infrared spectroscopy (FTIR)

FTIR spectra were measured with a Bruker Tensor 27 FTIR instrument (Bruker Optics) equipped with an MCT detector cooled with liquid nitrogen. 300 μl each of the QUIC samples (30 μg of rPrP) were pelleted by centrifugation for 1 h at 77,000 *g*, and resuspended in 20 μl buffer (300 mM NaCl, 50 mM HEPES pH 7.5). The slurry was loaded into BioATRcell II. PrP^{Sc} was purified from the brains of mice infected with the mouse-adapted Chandler and 22L prion using a combination of detergent solubilization, centrifugation at ultrahigh speeds and PK digestion (4, 32), and 15 μl of purified PrP^{Sc} were directly loaded. 128 scans at 4 cm^{-1} resolution were collected for each sample under constant purging with nitrogen, corrected for water vapor, and background spectra of buffer were subtracted.

198

199 **Conformational stability assay**

200 10 μl of the QUIC products (equivalent to 1 μg of rPrP) and brain homogenates (80 μg of
201 total proteins) were mixed with 22 μl of various concentrations of guanidine
202 hydrochloride (GdnHCl) at a final concentration of 0 to 5 M and 0 to 3.5 M, respectively,
203 and the mixed samples were incubated at 37 ºC for 1h. After adjusting the final GdnHCl
204 concentration of the QUIC products to 1 M and the brain homogenates to 0.6 M, the
205 samples were digested with PK (10 μg/ml) at 37 ºC for 1h, and analyzed by Western
206 blotting following methanol precipitation. The bands were visualized using Attophos AP
207 Fluorescent Substrate system (Promega) and quantified using Molecular Imager FX
208 (BIO-RAD). The sigmoidal patterns of denaturation curves were plotted using a
209 Boltzmann curve fit. The concentration of GdnHCl required to denature 50% of
210 PK-resistant fragments ($[GdnHCl]_{1/2}$) was estimated from the denaturation curves.

211

212 **Bioassay**

213 Male 4-week-old ddY mice were intracerebrally inoculated with 40 μl of QUIC products

(equivalent to 4 μg rPrP). As controls for rPrP-fibrils, we performed a mock QUIC procedure using seed-only solutions that contained the same concentration of PrP^{Sc} as 1^{st}--rPrP-fibril (1 pg/μl) or 5^{th}-rPrP-fibril (1×10^{-8} pg/μl), then added the same amount of rPrP, and inoculated the mixtures into mice. Brain homogenates were serially diluted with PBS, from 10^{0} to 10^{-7}, and 20 μl of each dilution was intracerebrally inoculated. Mice were monitored weekly until the terminal stage of disease or sacrifice. Clinical onset was determined as the presence of 3 or more of the following signs: greasy and/or yellowish hair, hunchback, weight loss, yellow pubes, ataxic gait and nonparallel hind limbs. The 50% lethal dose (LD_{50}) was determined according to the Behrens-Karber formula. Animals were cared for in accordance with the Guidelines for Animal Experimentation of Nagasaki University.

Histopathology and Lesion Profiles

The brain tissue was fixed in 4% paraformaldehyde, and 5 μm paraffin sections prepared on PLL coat slides using a microtome. After deparaffinization and rehydration, the tissue sections were stained with hematoxylin and eosin. The pattern of vacuolation was

examined in 8 fields per slice from the hippocampus, cerebral cortex, hypothalamus, pons and cerebellum. Spongiform degeneration was scored using the following scale: 0, no vacuoles; 1, a few vacuoles widely and unevenly distributed; 2, a few vacuoles evenly scattered; 3, moderate numbers of vacuoles evenly scattered; 4, many vacuoles with some confluences; 5, dense vacuolation.

Statistical Analysis

The fibril-length or width determined by electron microscopy analysis was subjected to one-way analysis of variance (ANOVA) followed by Tukey-Kramer test. The data of the conformational stability test was analyzed by one-way ANOVA followed by student's *t*-test. The data analysis of the survival times was evaluated by Logrank test. The data of the vacuolation score was analyzed by Mann-Whitney's U test.

Results

Conversion of the soluble form of mouse recombinant PrP into amyloid fibrils by RT-QUIC

We first tested whether formation of mouse rPrP amyloid fibrils could be induced in the RT-QUIC by monitoring levels of ThT fluorescence. We observed positive ThT fluorescence in the presence of diluted Chandler-brain homogenate (BH) or 22L-BH containing 100 pg of PrP^{Sc} (Fig. 1A), whereas negative control reactions seeded with comparable dilutions of normal brain homogenate (NBH) or without seed resulted in no increase in ThT fluorescence over 72 h (Fig. 1A). However, because an inverse correlation existed between the rate of fibril formation and the concentration of rPrP (28, 33), spontaneous formation of rPrP-fibrils (rPrP-fib^{spon}) was induced by decreasing the concentration of rPrP from 100 to 50 μg/ml (Fig. 1A).

We next examined the PK-resistance of rPrP-fibrils by immunoblotting using anti-PrP antibody R20 directed toward C-terminal residues 218–231. Although the ThT-negative reactions seeded with NBH or without seed produced no PK-resistant bands (Fig. 1B middle panel), the Chandler-seeded rPrP-fibrils (rPrP-fib^{Ch}) and

22L-seeded rPrP-fibrils (rPrP-fib^{22L}) produced several (21-, 18-, 12-, 11-and 10-kDa) PK-resistant fragments (Fig. 1B, left panel). In contrast, the PK digestion of rPrP-fib^{spon} generated only 10-12 kDa fragments. It should be noted that anti-PrP monoclonal antibody ICSM35 (directed toward an epitope consisting of residues 93-102) specifically recognized the 21- and 18 kDa fragments derived from PrP^{Sc}-seeded rPrP-fibrils in the first round (1st-rPrP-fib^{Sc}), indicating that they contained mouse PrP from about residues 93-231 (Fig. 1B, right panel).

To further characterize the structure of 1st-rPrP-fib^{Sc} and rPrP-fib^{spon}, the samples were examined using a negative-stained transmission electron microscope (TEM). The electron micrographs of 1st-rPrP-fib^{Ch} and 1st-rPrP-fib^{22L} revealed bundles of irregularly rod-shaped and branched fibrils, while most rPrP-fib^{spon} displayed smooth and non-branched rod-shaped fibrils (Fig. 1C). Moreover, the lengths of 1st-rPrP-fib^{Ch} and 1st-rPrP-fib^{22L} were significantly longer than that of rPrP-fib^{spon} (Fig. 1D). Thus, the results of TEM analysis suggest that 1st-rPrP-fib^{Sc} is structurally distinct from spontaneous rPrP-fib^{spon}.

We next examined the morphology of PrP^{Sc}-seeded rPrP-fibrils in the second

and fifth round reactions (2^{nd}- and 5^{th}-rPrP-fib^{Sc}) by TEM. In contrast to 1^{st}-rPrP-fib^{Sc}, 2^{nd}- and 5^{th}-rPrP-fib^{Sc} displayed spindly and non-branched fibrils or amorphous aggregates (Fig. 2). These data support the view that 1^{st}-rPrP-fib^{Sc} are structurally distinct from those of 2^{nd}- and 5^{th}-rPrP fib^{Sc}.

Structural characterization of rPrP-fibrils by FTIR

We next examined the secondary structure of rPrP-fibrils and purified PrP^{Sc} from brains of mice infected with Chandler or 22L scrapie by FTIR. A silver-stained SDS-PAGE gel analysis revealed that Chandler- and 22L-PrP^{Sc} preparations were highly purified (Fig. 3A). Furthermore, TEM analysis demonstrated that the PrP^{Sc} preparations consisted exclusively of amyloid-like fibrils (Fig. 3B). FTIR analysis showed that Chandler-PrP^{Sc} was characterized by a major band at 1630 cm^{-1} in the β-sheet region of second-derivative spectra, while 22L-PrP^{Sc} was characterized by two absorbance bands at 1631 and 1616 cm^{-1} (Fig. 4A), indicating that there were conformational differences in β-sheet structures between Chandler- and 22L-PrP^{Sc}, as previously reported (7). Consistent with previous reports (6-9), bands of around 1656–1658 cm^{-1} were observed in both Chandler- and

22L-PrP^{Sc}. Although these bands were formerly attributed to α-helix, recent studies using direct mass spectrometric analysis of hydrogen/deuterium exchange and FTIR analysis have suggested that purified PrP^{Sc} has little α-helix content, and the bands probably result from turns (9, 34). Native rPrP had maximum absorbance at 1653 cm^{-1}, which was congruent with that of prominent α-helical structures. In contrast, all rPrP-fibrils displayed prominent bands at lower wavenumbers (1630-1610 cm^{-1}), indicating predominantly β-sheet content (Fig. 4A). The β-sheet spectra revealed conformational differences among rPrP-fib^{spon}, 1^{st}-rPrP-fib^{Ch} and 1^{st}-rPrP-fib^{22L}. The rPrP-fib^{spon} had a prominent band at 1623 cm^{-1} and a modest band at 1610 cm^{-1}. While the 1^{st}-rPrP-fib^{Ch} was characterized by a single major band at 1624 cm^{-1}, the 1^{st}-rPrP-fib^{22L} had two major maxima at 1629 and 1617 cm^{-1} (Fig. 4A). Although 1^{st}-rPrP-fib^{Sc} lacked the bands around 1656–1658 cm^{-1}, the strain-specific shapes (one peak in Chandler versus two peaks in 22L) in the β-sheet spectrum of the purified PrP^{Sc} resembled those of 1^{st}-rPrP-fib^{Sc}.

To test whether the strain-specific IR spectra observed in 1^{st}-rPrP-fib^{Ch} and 1^{st}-rPrP-fib^{22L} are transmitted to sequential QUIC reactions, we performed 5 serial rounds of QUIC (Supplementary Fig. 2). There was little difference in β-sheet spectra between

307 5^{th}-rPrP-fib^{Ch} and 5^{th}-rPrP-fib^{22L} (Fig 3), suggesting that strain-specific conformations

308 were lost in the 5^{th}-rPrP-fib^{Sc}. Furthermore, additional experiments revealed that infrared

309 spectra of rPrP-fibrils produced in the presence of low amount of PrP^{Sc} (1 pg) or under

310 acidic conditions (pH 4) displayed little differences between strains (Fig. 4B).

311

312 **Conformational stability analysis of rPrP-fibrils and PrP^{Sc}**

313 To examine the biochemical differences of rPrP-fibrils and PrP^{Sc} in BH

314 between strains, we performed a conformational stability assay, which combines GdnHCl

315 denaturation with PK digestion. The $[GdnHCl]_{1/2}$ values for Chandler- and 22L-PrP^{Sc}

316 were 3.3 ± 0.4 and 1.7 ± 0.3 M, respectively (Fig. 5A and Table 1), indicating that the

317 conformational stability of Chandler-PrP^{Sc} was significantly higher than that of

318 22L-PrP^{Sc}. Consistent with previous work (11), Chandler-PrP^{Sc} bands treated with more

319 than 1.5 M GdnHCl were approximately 5 kDa smaller than those treated with lower

320 concentrations (Fig. 5A, upper panel). The $[GdnHCl]_{1/2}$ of 1^{st}-rPrP-fib^{Ch} and

321 1^{st}-rPrP-fib^{22L} were 3.3 ± 0.1 and 2.3 ± 0.6 M, respectively (Fig. 5B and Table 1),

322 showing that the stability of 1^{st}-rPrP-fib^{Ch} was significantly higher than that of

323 1^{st}-rPrP-fib^{22L}, as with Chandler- and 22L-PrP^{Sc}. Thus, the relationship between Chandler

324 and 22L in terms of conformational stability was common to both the original PrP^{Sc} and

325 1^{st}-rPrP-fib^{Sc}. In contrast, the $[GdnHCl]_{1/2}$ of rPrP-fib^{spon} was more than 5 M, which was

326 markedly higher than those of the 1^{st}-rPrP-fib^{Sc} (Fig. 5B and Table 1). Additionally, we

327 tested the conformational stability of 2^{nd}- and 5^{th}-rPrP-fib^{Sc}, but found no significant

328 differences between strains (Fig. 5C, D and Table 1).

329

330 **Bioassay for rPrP-fibrils generated in QUIC reactions**

331 To determine whether the infectivity was transmitted to the rPrP-fibrils, we

332 performed a bioassay using wild-type mice. To prepare the control materials, seed-only

333 solutions containing the same concentration of PrP^{Sc} as 1^{st}- or 5^{th}-rPrP-fib^{Sc} were

334 subjected to a mock RT-QUIC procedure and then mixed with the same amount of

335 soluble rPrP (Table 2). The survival periods in mice inoculated with 40 μl aliquots

336 containing rPrP-fibrils were 185.5 ± 4.0 days post-inoculation (dpi) for 1^{st}-rPrP-fib^{Ch} and

337 213.0 ± 8.9 dpi for 1^{st}-rPrP-fib^{22L} (Table 2). In contrast, the attack rate of these control

338 mice was only 50% (2/4) for Chandler and 20% (1/5) for 22L. Moreover, the survival

periods of the affected mice were much longer than that of the mice inoculated with 1^{st}-rPrP-fib^{Sc} (Table 2). For comparison with the 50% lethal dose (LD_{50}) of the original PrP^{Sc}, the LD_{50} of 1^{st}-rPrP-fib^{Sc} was determined by the linear regression relationship between infectious titers and survival periods. The infectious titers (per 40 μl) of 1^{st}-rPrP-fib^{Ch} and 1^{st}-rPrP-fib^{22L} were estimated to be 407.2 ± 226.6 and 1067.0 ± 678.7 LD_{50}, respectively, whereas the titers of Chandler and 22L prion were 20.2 and 28.9 LD_{50} units/40 pg of PrP^{Sc}, respectively. Because QUIC reaction in the first round resulted in a 20- to 37-fold increase in the infectious titer, a seed contribution to the infectivity is estimated to be around 3−5%. In contrast, none of the mice inoculated with 5^{th}-rPrP-fib^{Sc} developed symptoms related to TSE (Table 2), suggesting that the 5^{th}-rPrP-fib^{Sc} has no substantial infectivity.

We analyzed the levels of PrP^{Sc} in the brain tissues of terminal-stage mice inoculated with 1^{st}-rPrP-fib^{Sc} or control materials (Mock 1^{st}-QUIC) by Western blotting and found no apparent differences in the accumulation of PrP^{Sc} between them and the Mock 1^{st}-QUIC (Fig. 6A). In addition, a conformational stability assay with GdnHCl revealed that the strain-specific digestion pattern was preserved in mice inoculated with

355 1^{st}-rPrP-fib^{Sc} (Fig. 6B).

356 Next, the degree of vacuolation in brain sections including the hippocampus
357 (HI), cerebral cortex (Cx), thalamus (TH), pons (Po) and cerebellum (CE) from affected
358 mice inoculated with 1^{st}-rPrP-fib^{Sc} or Mock 1^{st}-QUIC and those in the second passage of
359 1^{st}-rPrP-fib^{Sc} was examined histologically (Fig. 6C, D). Of note, we found that
360 spongiform change of 1^{st}-rPrP-fib^{Sc}-inoculated mice was less severe in HI and CE than
361 that of Mock 1^{st}-QUIC (Fig. 6C, D). Furthermore, these different lesion profiles observed
362 in 1^{st}-rPrP-fib^{Sc}-inoculated mice were preserved upon second passage (Fig. 6D),
363 suggesting that 1^{st}-rPrP-fib^{Sc} are partially distinct from the original strains. These
364 findings support the notion that 1^{st}-rPrP-fib^{Sc} provoke the emergence of a mutant strain
365 beyond seed-derived infectivity.

366

367 **DISCUSSION**

368 Recent studies show that RT-QUIC assays are useful for the sensitive detection
369 of PrP^{Sc} in most species and strains, including Creutzfeldt-Jakob disease (CJD) in humans
370 (28, 35-37), scrapie in rodents (29, 38), and chronic wasting disease (CWD) in cervids

371 (39). In the RT-QUIC reaction, soluble rPrP is converted to amyloid fibrils in a
372 seed-dependent fashion in the presence of PrP^{Sc}. Previous studies using FTIR and
373 hydrogen/deuterium exchange have shown that there are structural differences between
374 PrP^{Sc}-seeded and spontaneous rPrP-fibrils generated in the rPrP-PMCA (7, 40). We also
375 found that the structural morphology (Fig. 1C), secondary structure (Fig. 3) and
376 conformational stability (Fig. 4B and Table 1) distinguish 1^{st}-rPrP-fib^{Sc} from rPrP-fib^{spon}.
377 However, it has been unknown whether rPrP retains the conformational properties of the
378 original PrP^{Sc} in the RT-QUIC. Consistent with previous reports (7, 11), we observed
379 strain differences in β-sheet structure and conformational stability of PrP^{Sc} between
380 Chandler and 22L strains. Likewise, the differences in β-sheet spectrum shape between
381 strains were common to both PrP^{Sc} and 1^{st}-rPrP-fib^{Sc}. Furthermore, the conformational
382 stability of 1^{st}-rPrP-fib^{22L} was significantly lower than that of 1^{st}-rPrP-fib^{Ch}, as with
383 Chandler- and 22L-PrP^{Sc}. Since the original PrP^{Sc} remaining in the 1^{st}-rPrP-fib^{Sc} was
384 equivalent to only about 0.01−0.02% of PK-resistant 1^{st}-rPrP-fib^{Sc} (1−2 μg/10 μg of total
385 PrP) in our estimation, the contribution to the FTIR spectra and the conformational
386 stability of 1^{st}-rPrP-fib^{Sc} is considered to be negligible. Taken together, these studies

387 demonstrate that at least some strain-specific conformational features, especially in the
388 β-sheet region, are conserved between PrP^{Sc} and 1^{st}-rPrP-fib^{Sc}. However, these unique
389 structural features disappeared in subsequent rounds.

390 One of the reasons for the loss of strain-specificity may be due to differences
391 between *E. coli*-derived rPrP and brain-derived PrP^{C}. Studies using circular dichroism
392 and ^{1}H-NMR spectroscopy showed that the tertiary structure and the thermal stability of
393 bovine rPrP(23-230) are essentially identical to those of healthy calf brain-derived PrP^{C}
394 (41). However, it should be noted that *E. coli*-derived rPrP lacks posttranslational
395 modifications of PrP^{C} such as glycosylation and a glycosylphosphatidylinositol
396 (GPI)-anchor. PrP has two N-linked glycosylation sites at amino acids 180 and 196,
397 resulting in di-, mono- and unglycosylated forms. Mature PrP^{C} is rich in the
398 di-glycosylated form, whereas the glycoform ratio of PrP^{Sc} is known to vary among
399 strains (42-44). Studies using PrP glycan-lacking Tg mice revealed that the
400 strain-specific characteristics of 79A strain were affected in by the glycosylation status of
401 PrP^{C}, but ME7 and 301C strains were not (45). Meanwhile, enzymatic deglycosylation of
402 PrP^{C} failed to affect strain-specific pathological changes in serial PMCA experiments

403 seeded with two murine strains, RML and 301C (46). However, the same two strains
404 were converted into a new single strain during serial rPrP-PMCA in the presence of
405 synthetic PE (27). Similarly, the emergence of mutant strains whose lesion profiles differ
406 from that of the seed strain was also observed in the bioassay using hamster rPrP-fibrils
407 generated in seeded rPrP-PMCA (25) or 1^{st}-rPrP-fib^{Sc} (Fig. 6C, D). These results raise the
408 possibility that the lack of a GPI-anchor in rPrP leads to alterations in the strain-specific
409 characteristics. Furthermore, the cell tropisms determined by the Cell Panel Assay were
410 altered in RML, 139A, 79A and ME7 strains but not in 22L when propagated in Tg mice
411 expressing PrP devoid of a GPI-anchor (47). These studies demonstrate that
412 glycosylation and a GPI-anchor are not necessarily required for the propagation of prion
413 infectivity, but can influence the strain properties. Although the molecular basis of the
414 emergence of mutant strains remains elusive, we can speculate that the posttranslational
415 changes to PrP might affect the conformation of PrP^{Sc} or the interaction with some
416 cofactor(s) in a strain-specific manner.
417 Another possible explanation is that nonspecific rPrP-fibrils are generated
418 during the serial RT-QUIC, and replicate more rapidly than the fibrils with strain-specific

419 conformation. The term “nonspecific rPrP-fibrils” arises from our findings that there was
420 little difference in IR spectra and conformational stability of 5^{th}-rPrP-fib^{Sc} between
421 strains. It has been reported that the propagation of prion strains in cells cultured under
422 different environments often leads to the formation of quasi-species that are assumed to
423 be composed of a variety of conformational variants (48, 49). Once generated, the
424 competition among the variants is thought to occur during propagation. Indeed, two
425 conformational variants of rPrP-fibrils have been shown to be mutually exclusive and
426 compete for monomeric rPrP as a substrate in the fibril formation (30). Furthermore,
427 competitive amplification of two prion strains was demonstrated by BH-PMCA (50).
428 Similarly, nonspecific rPrP-fibrils would be expected to become the majority if they had a
429 selective growth advantage in the RT-QUIC. We found that the β-sheet spectra of
430 rPrP-fibrils generated in the presence of low amount (1 pg) of PrP^{Sc} or rPrP-fibrils
431 generated at pH 4 in the first round were similar to those seen in 5^{th}-rPrP-fib^{Sc} (Fig. 4B).
432 These observations also support this hypothesis and suggest that the amplification of
433 nonspecific rPrP-fibrils is accelerated by certain conditions such as an acidic environment.
434 Further studies are needed to investigate whether unknown cofactors or environmental

conditions are required to maintain the strain-specific conformations in subsequent rounds. On the other hand, this hypothesis also explains why prion infectivity was lost in the fifth round of RT-QUIC, as nonspecific rPrP-fibrils generated during the serial RT-QUIC would be non-infectious. Although there remains the question as to what exactly are the conformational differences between the non-infectious and infectious forms of rPrP-fibrils, the lack of cofactor molecules such as SDS and synthetic PE in the RT-QUIC might enhance the amplification of nonspecific rPrP-fibrils lacking prion infectivity. Moreover, the facts that prion infectivity is sometimes too low to be detected and, more frequently, declines in the serial rPrP-PMCA (24, 25) or BH-PMCA (51-53) are consistent with the hypothesis.

ACKNOWLEDGMENTS

We thank Takashi Suematsu for help with the electron microscopy study, and Matsuo Atsuko and Ayumi Yamakawa for technical assistance.

This work was supported by a grant-in-aid for young scientists (B; grant no. 21790846) from the Ministry of Education, Culture, Sports, Science and Technology of

Japan, a grant for BSE research, and a grant-in-aid of the Research Committee of Prion Disease and Slow Virus Infection from the Ministry of Health, Labor and Welfare of Japan.

References

1. **Prusiner SB.** 1991. Molecular biology of prion diseases. Science **252:**1515-1522.

2. **Weissmann C, Enari M, Klohn PC, Rossi D, Flechsig E.** 2002. Molecular biology of prions. Acta Neurobiol Exp (Wars) **62:**153-166.

3. **Meyer RK, McKinley MP, Bowman KA, Braunfeld MB, Barry RA, Prusiner SB.** 1986. Separation and properties of cellular and scrapie prion proteins. Proc Natl Acad Sci U S A **83:**2310-2314.

4. **Caughey BW, Dong A, Bhat KS, Ernst D, Hayes SF, Caughey WS.** 1991. Secondary structure analysis of the scrapie-associated protein PrP 27-30 in water by infrared spectroscopy. Biochemistry **30:**7672-7680.

5. **Pan KM, Baldwin M, Nguyen J, Gasset M, Serban A, Groth D, Mehlhorn I, Huang Z, Fletterick RJ, Cohen FE, Prusiner SB.** 1993. Conversion of alpha-helices into beta-sheets features in the formation of the scrapie prion proteins. Proc Natl Acad Sci U S A **90:**10962-10966.

6. **Caughey B, Raymond GJ, Bessen RA.** 1998. Strain-dependent differences in beta-sheet conformations of abnormal prion protein. J Biol Chem

273:32230-32235.

7. **Atarashi R, Sim VL, Nishida N, Caughey B, Katamine S.** 2006. Prion strain-dependent differences in conversion of mutant prion proteins in cell culture. J Virol **80:**7854-7862.

8. **Thomzig A, Spassov S, Friedrich M, Naumann D, Beekes M.** 2004. Discriminating scrapie and bovine spongiform encephalopathy isolates by infrared spectroscopy of pathological prion protein. J Biol Chem **279:**33847-33854.

9. **Baron GS, Hughson AG, Raymond GJ, Offerdahl DK, Barton KA, Raymond LD, Dorward DW, Caughey B.** 2011. Effect of glycans and the glycophosphatidylinositol anchor on strain dependent conformations of scrapie prion protein: improved purifications and infrared spectra. Biochemistry **50:**4479-4490.

10. **Peretz D, Scott MR, Groth D, Williamson RA, Burton DR, Cohen FE, Prusiner SB.** 2001. Strain-specified relative conformational stability of the scrapie prion protein. Protein Sci **10:**854-863.

11. **Shindoh R, Kim CL, Song CH, Hasebe R, Horiuchi M.** 2009. The region approximately between amino acids 81 and 137 of proteinase K-resistant PrPSc is critical for the infectivity of the Chandler prion strain. J Virol **83:**3852-3860.

12. **Saborio GP, Permanne B, Soto C.** 2001. Sensitive detection of pathological prion protein by cyclic amplification of protein misfolding. Nature **411:**810-813.

13. **Castilla J, Saa P, Hetz C, Soto C.** 2005. In vitro generation of infectious scrapie prions. Cell **121:**195-206.

14. **Castilla J, Morales R, Saa P, Barria M, Gambetti P, Soto C.** 2008. Cell-free propagation of prion strains. EMBO J **27:**2557-2566.

15. **Deleault NR, Harris BT, Rees JR, Supattapone S.** 2007. Formation of native prions from minimal components in vitro. Proc Natl Acad Sci U S A **104:**9741-9746.

16. **Imamura M, Kato N, Yoshioka M, Okada H, Iwamaru Y, Shimizu Y, Mohri S, Yokoyama T, Murayama Y.** 2011. Glycosylphosphatidylinositol anchor-dependent stimulation pathway required for generation of baculovirus-derived recombinant scrapie prion protein. J Virol **85:**2582-2588.

17. **Imamura M, Kato N, Okada H, Yoshioka M, Iwamaru Y, Shimizu Y, Mohri S, Yokoyama T, Murayama Y.** 2013. Insect Cell-Derived Cofactors Become Fully Functional after Proteinase K and Heat Treatment for High-Fidelity Amplification of Glycosylphosphatidylinositol-Anchored Recombinant Scrapie and BSE Prion Proteins. PLoS One **8:**e82538.

18. **Legname G, Baskakov IV, Nguyen HO, Riesner D, Cohen FE, DeArmond SJ, Prusiner SB.** 2004. Synthetic mammalian prions. Science **305:**673-676.

19. **Colby DW, Giles K, Legname G, Wille H, Baskakov IV, DeArmond SJ, Prusiner SB.** 2009. Design and construction of diverse mammalian prion strains. Proc Natl Acad Sci U S A **106:**20417-20422.

20. **Raymond GJ, Race B, Hollister JR, Offerdahl DK, Moore RA, Kodali R, Raymond LD, Hughson AG, Rosenke R, Long D, Dorward DW, Baron GS.** 2012. Isolation of novel synthetic prion strains by amplification in transgenic mice coexpressing wild-type and anchorless prion proteins. J Virol **86:**11763-11778.

21. **Makarava N, Kovacs GG, Bocharova O, Savtchenko R, Alexeeva I, Budka H,**

Rohwer RG, Baskakov IV. 2010. Recombinant prion protein induces a new transmissible prion disease in wild-type animals. Acta Neuropathol **119:**177-187.

22. **Wang F, Wang X, Yuan CG, Ma J.** 2010. Generating a prion with bacterially expressed recombinant prion protein. Science **327:**1132-1135.

23. **Zhang Z, Zhang Y, Wang F, Wang X, Xu Y, Yang H, Yu G, Yuan C, Ma J.** 2013. De novo generation of infectious prions with bacterially expressed recombinant prion protein. FASEB J **27:**4768-4775.

24. **Timmes AG, Moore RA, Fischer ER, Priola SA.** 2013. Recombinant prion protein refolded with lipid and RNA has the biochemical hallmarks of a prion but lacks in vivo infectivity. PLoS One **8:**e71081.

25. **Kim JI, Cali I, Surewicz K, Kong Q, Raymond GJ, Atarashi R, Race B, Qing L, Gambetti P, Caughey B, Surewicz WK.** 2010. Mammalian prions generated from bacterially expressed prion protein in the absence of any mammalian cofactors. J Biol Chem **285:**14083-14087.

26. **Deleault NR, Piro JR, Walsh DJ, Wang F, Ma J, Geoghegan JC, Supattapone S.** 2012. Isolation of phosphatidylethanolamine as a solitary cofactor for prion

formation in the absence of nucleic acids. Proc Natl Acad Sci U S A **109:**8546-8551.

27. **Deleault NR, Walsh DJ, Piro JR, Wang F, Wang X, Ma J, Rees JR, Supattapone S.** 2012. Cofactor molecules maintain infectious conformation and restrict strain properties in purified prions. Proc Natl Acad Sci U S A **109:**E1938-1946.

28. **Atarashi R, Satoh K, Sano K, Fuse T, Yamaguchi N, Ishibashi D, Matsubara T, Nakagaki T, Yamanaka H, Shirabe S, Yamada M, Mizusawa H, Kitamoto T, Klug G, McGlade A, Collins SJ, Nishida N.** 2011. Ultrasensitive human prion detection in cerebrospinal fluid by real-time quaking-induced conversion. Nat Med **17:**175-178.

29. **Wilham JM, Orru CD, Bessen RA, Atarashi R, Sano K, Race B, Meade-White KD, Taubner LM, Timmes A, Caughey B.** 2010. Rapid end-point quantitation of prion seeding activity with sensitivity comparable to bioassays. PLoS Pathog **6:**e1001217.

30. **Atarashi R, Moore RA, Sim VL, Hughson AG, Dorward DW, Onwubiko HA,**

552 **Priola SA, Caughey B.** 2007. Ultrasensitive detection of scrapie prion protein
553 using seeded conversion of recombinant prion protein. Nat Methods **4:**645-650.
554 31. **Fujihara A, Atarashi R, Fuse T, Ubagai K, Nakagaki T, Yamaguchi N,**
555 **Ishibashi D, Katamine S, Nishida N.** 2009. Hyperefficient PrP Sc amplification
556 of mouse-adapted BSE and scrapie strain by protein misfolding cyclic
557 amplification technique. FEBS J **276:**2841-2848.
558 32. **Kocisko DA, Lansbury PT, Jr., Caughey B.** 1996. Partial unfolding and
559 refolding of scrapie-associated prion protein: evidence for a critical 16-kDa
560 C-terminal domain. Biochemistry **35:**13434-13442.
561 33. **Atarashi R, Sano K, Satoh K, Nishida N.** 2011. Real-time quaking-induced
562 conversion: a highly sensitive assay for prion detection. Prion **5:**150-153.
563 34. **Smirnovas V, Baron GS, Offerdahl DK, Raymond GJ, Caughey B, Surewicz**
564 **WK.** 2011. Structural organization of brain-derived mammalian prions examined
565 by hydrogen-deuterium exchange. Nat Struct Mol Biol **18:**504-506.
566 35. **McGuire LI, Peden AH, Orru CD, Wilham JM, Appleford NE, Mallinson G,**
567 **Andrews M, Head MW, Caughey B, Will RG, Knight RS, Green AJ.** 2012.

568 Real time quaking-induced conversion analysis of cerebrospinal fluid in sporadic
569 Creutzfeldt-Jakob disease. Ann Neurol **72:**278-285.
570 36. **Orru CD, Wilham JM, Raymond LD, Kuhn F, Schroeder B, Raeber AJ,**
571 **Caughey B.** 2011. Prion disease blood test using immunoprecipitation and
572 improved quaking-induced conversion. MBio **2:**e00078-00011.
573 37. **Sano K, Satoh K, Atarashi R, Takashima H, Iwasaki Y, Yoshida M, Sanjo N,**
574 **Murai H, Mizusawa H, Schmitz M, Zerr I, Kim YS, Nishida N.** 2013. Early
575 detection of abnormal prion protein in genetic human prion diseases now possible
576 using real-time QUIC assay. PLoS One **8:**e54915.
577 38. **Vascellari S, Orru CD, Hughson AG, King D, Barron R, Wilham JM, Baron**
578 **GS, Race B, Pani A, Caughey B.** 2012. Prion seeding activities of mouse scrapie
579 strains with divergent PrPSc protease sensitivities and amyloid plaque content
580 using RT-QuIC and eQuIC. PLoS One **7:**e48969.
581 39. **Henderson DM, Manca M, Haley NJ, Denkers ND, Nalls AV, Mathiason CK,**
582 **Caughey B, Hoover EA.** 2013. Rapid antemortem detection of CWD prions in
583 deer saliva. PLoS One **8:**e74377.

584 40. **Smirnovas V, Kim JI, Lu X, Atarashi R, Caughey B, Surewicz WK.** 2009.
585 Distinct structures of scrapie prion protein (PrPSc)-seeded versus spontaneous
586 recombinant prion protein fibrils revealed by hydrogen/deuterium exchange. J
587 Biol Chem **284:**24233-24241.
588 41. **Hornemann S, Schorn C, Wuthrich K.** 2004. NMR structure of the bovine
589 prion protein isolated from healthy calf brains. EMBO Rep **5:**1159-1164.
590 42. **Clarke AR, Jackson GS, Collinge J.** 2001. The molecular biology of prion
591 propagation. Philos Trans R Soc Lond B Biol Sci **356:**185-195.
592 43. **Lawson VA, Collins SJ, Masters CL, Hill AF.** 2005. Prion protein glycosylation.
593 J Neurochem **93:**793-801.
594 44. **Aguzzi A, Heikenwalder M, Polymenidou M.** 2007. Insights into prion strains
595 and neurotoxicity. Nat Rev Mol Cell Biol **8:**552-561.
596 45. **Cancellotti E, Mahal SP, Somerville R, Diack A, Brown D, Piccardo P,**
597 **Weissmann C, Manson JC.** 2013. Post-translational changes to PrP alter
598 transmissible spongiform encephalopathy strain properties. EMBO J **32:**756-769.
599 46. **Piro JR, Harris BT, Nishina K, Soto C, Morales R, Rees JR, Supattapone S.**

2009. Prion protein glycosylation is not required for strain-specific neurotropism. J Virol **83:**5321-5328.

47. **Mahal SP, Jablonski J, Suponitsky-Kroyter I, Oelschlegel AM, Herva ME, Oldstone M, Weissmann C.** 2012. Propagation of RML prions in mice expressing PrP devoid of GPI anchor leads to formation of a novel, stable prion strain. PLoS Pathog **8:**e1002746.

48. **Li J, Browning S, Mahal SP, Oelschlegel AM, Weissmann C.** 2010. Darwinian evolution of prions in cell culture. Science **327:**869-872.

49. **Weissmann C, Li J, Mahal SP, Browning S.** 2011. Prions on the move. EMBO Rep **12:**1109-1117.

50. **Shikiya RA, Ayers JI, Schutt CR, Kincaid AE, Bartz JC.** 2010. Coinfecting prion strains compete for a limiting cellular resource. J Virol **84:**5706-5714.

51. **Bieschke J, Weber P, Sarafoff N, Beekes M, Giese A, Kretzschmar H.** 2004. Autocatalytic self-propagation of misfolded prion protein. Proc Natl Acad Sci U S A **101:**12207-12211.

52. **Klingeborn M, Race B, Meade-White KD, Chesebro B.** 2011. Lower specific

infectivity of protease-resistant prion protein generated in cell-free reactions. Proc Natl Acad Sci U S A **108:**E1244-1253.

53. **Gonzalez-Montalban N, Lee YJ, Makarava N, Savtchenko R, Baskakov IV.** 2013. Changes in prion replication environment cause prion strain mutation. FASEB J **27:**3702-3710.

FIGURE LEGENDS

FIGURE 1. The formation of rPrP-fibrils in RT-QUIC reactions. (A) The formation of rPrP-fibrils in the presence of diluted Chandler- or 22L-BH containing 100 pg of PrP^{Sc}, a comparable amount of NBH, or in the absence of seed (No-seeded) was monitored by ThT fluorescence. The graphs depict a representative of the RT-QUIC reactions. No-seeded reactions were performed at two different concentrations (100 or 50 μg/ml) of rPrP. (B) The QUIC reactions were digested with PK and immunoblotted using polyclonal anti-PrP antibody R20 (epitope located at mouse PrP amino acids 218-231) or ICSM35 (epitope 93-102). For comparison, 1^{st}-rPrP-fib^{Ch} (50 ng of total rPrP) without PK digestion (PK (−)) is shown. Molecular mass markers are indicated in kilodaltons (kDa) on the left side of each panel. (C) Samples (1^{st}-rPrP-fib^{Ch}, 1^{st}-rPrP-fib^{22L} and rPrP-fib^{spon}) were examined with transmission electron microscopy (TEM). Scale bar, 100 nm. (D) The bar graph shows the length and width of rPrP-fib^{spon}, 1^{st}-rPrP-fib^{Ch} and 1^{st}-rPrP-fib^{22L}. The results are the mean ± SD of thirty rPrP-fibrils each. Statistical significance was determined using one-way analysis of variance (ANOVA) followed by Tukey-Kramer test. *, $p < 0.01$.

639

640 **FIGURE 2.** The formation of PrP^{Sc}-seeded rPrP-fibrils in the second (2^{nd}-rPrP-fib^{Sc}) and

641 fifth rounds (5^{th}-rPrP-fib^{Sc}) of RT-QUIC. (A) The former reactions were diluted 100-fold

642 into fresh rPrP between each round. The reaction buffer contained 300 mM NaCl, 50 mM

643 HEPES (pH7.5) and 10 μM ThT. The rPrP concentration was 100 μg/ml. (B)

644 Transmission electron microscopic analysis of PrP^{Sc}-seeded rPrP-fibrils generated in the

645 second, and fifth rounds of RT-QUIC. Scale bar, 100 nm.

646

647 **FIGURE 3.** Silver staining and Western blot analysis of purified PrP^{Sc}. (A) The purified

648 PrP^{Sc} samples (P) were examined by silver-stained SDS-PAGE gel analysis (left panel).

649 For comparison, the electrophoretic pattern of prion-infected brain homogenates (BH)

650 containing 100 μg total protein digested with PK (20 μg/ml, 37 ^{o}C for 1h) is shown (left

651 panel). The purified PrP^{Sc} samples (P) were immunoblotted with polyclonal anti-PrP

652 antibody M20 (right panel). Molecular mass markers (M) are indicated in kilodaltons

653 (kDa) on the left side of each panel. (B) Electron microscopy analysis of purified

654 22L-PrP^{Sc} (left panel) and Chandler-PrP^{Sc} (right panel). Scale bar, 100 nm.

FIGURE 4. FTIR spectroscopic characterization of rPrP-fibrils and purified PrP^{Sc}. (A) Second-derivative FTIR spectra are shown for purified PrP^{Sc}, 1^{st}-rPrP-fib^{Sc}, 5^{th}-rPrP-fib^{Sc}, spontaneous formation of rPrP-fibrils (rPrP-fib^{spon}), and native rPrP. Overlaid spectra are from independent preparations. (B) FTIR spectra of rPrP-fibrils generated at pH 7.5 in the presence of low amount (1 pg) of PrP^{Sc}, and rPrP-fibrils generated at pH 4 in the presence of 100 pg of PrP^{Sc}.

FIGURE 5. Conformational stability assay for PrP^{Sc} in BH and rPrP-fibrils. (A) Chandler- (upper panel) or 22L (lower panel)-infected BH was treated with 0 to 3.5 M GdnHCl and subjected to PK digestion. PrP^{Sc} was detected by R20 anti-PrP polyclonal antibody. The denaturation curves were plotted using Boltzmann curve fit (right panel). (B–D) PK-digested 1^{st}-rPrP-fib^{Sc} (generated as in Fig. 1) and rPrP-fib^{spon} (B), 2^{nd}-rPrP-fib^{Sc}(C), or 5^{th}-rPrP-fib^{Sc} (D) was analyzed by Western blotting following GdnHCl treatment (0 to 5M). The PK-resistant fragments of the rPrP-fibrils were detected by R20.

671

672 **FIGURE 6.** Bioassay of rPrP-fibrils in mice. (A) PrP^{Sc} in the brains of prion-affected
673 mice inoculated with 1^{st}-rPrP-fib^{Ch} or 1^{st}-rPrP-fib^{22L} was analyzed by Western blotting
674 using anti-PrP antibody M20. M, Mock 1^{st}-QUIC(Ch) or Mock 1^{st}-QUIC(22L). (B)
675 Strain-specific properties of PrP^{Sc} in the brains of 1^{st}-rPrP-fib^{Sc}-inoculated mice were
676 examined by a conformational stability assay with GdnHCl (0 to 3.5M). (C) Sections of
677 the hippocampus (HI)) and cerebellum (CE), stained with hematoxylin and eosin, from
678 normal mice, 1^{st}-rPrP-fib^{Sc}-inoculated mice, and Mock 1^{st}-QUIC-inoculated mice at
679 terminal stages are shown. Scale bar, 50 μm. (D) Lesion profiles of spongiform changes
680 in the hippocampus (HI), cerebral cortex (Cx), thalamus (TH), pons (Po) and cerebellum
681 (CE) were compared. Data are expressed as means ± SD (n=3). Statistical significance
682 was determined using Mann-Whitney's U test. **, $p < 0.01$; *, $p < 0.05$.

683

684 **TABLE 1.** Conformational stabilities of purified PrP^{Sc} and rPrP-fibrils[a]

Strain	Purified PrP^{Sc}	rPrP-fibrils		
		1st	2nd	5th
Chandler	3.3 ± 0.4 **	3.3 ± 0.1 *	3.7 ± 0.1	3.3 ± 0.3
22L	1.7 ± 0.3	2.3 ± 0.6	3.8 ± 0.2	3.5 ± 1.0
Spontaneous		> 5		

685 [a] The $[GdnHCl]_{1/2}$ values (mol/l) are means ± SD of three independent experiments.
686 Statistical significance was determined using one-way ANOVA followed by student's
687 *t*-test. **, $p < 0.01$; *, $p < 0.05$ (compared with 22L).

688

689

690 **TABLE 2.** Bioassay for rPrP-fibrils generated in QUIC reactions in wild-type mice[a]

Inoculum	Concentration of seed PrP^{Sc} (pg/μl)	Survival periods (dpi [b])	Mortality (no. dead/total)
1^{st}-rPrP-fib^{Ch}	1	185.5 ± 4.0* [d]	4/4
Mock 1^{st}-QUIC(Ch) [c]	1	201, 220 [e]	2/4
1^{st}-rPrP-fib^{22L}	1	213.0 ± 8.9** [d]	6/6
Mock 1^{st}-QUIC(22L) [c]	1	333 [e]	1/5
5^{th}-rPrP-fib^{Ch}	1×10^{-8}	> 660 [f]	0/4
Mock 5^{th}-QUIC(Ch) [c]	1×10^{-8}	> 660 [f]	0/4
5^{th}-rPrP-fib^{22L}	1×10^{-8}	> 660 [f]	0/6
Mock 5^{th}-QUIC(22L) [c]	1×10^{-8}	> 660 [f]	0/6
rPrP-fib^{spon}	0	> 660 [f]	0/6
Second passage of 1^{st}-rPrP-fib^{Ch}		152.0 ± 8.5 [d]	5/5
Second passage of Mock 1^{st}-QUIC(Ch) [g]		148.4 ± 5.9 [d]	5/5
Second passage of 1^{st}-rPrP-fib^{22L}		153.5 ± 0.6 [d]	5/5
Second passage of Mock 1^{st}-QUIC(22L) [h]		149.6 ± 10.4 [d]	4/4

691 [a] Mice were intracerebrally inoculated with 40 μl of each inoculum. For the second
692 passage, 10% BH was used. Statistical significance was determined using Logrank test.
693 **, $p < 0.01$; *, $p < 0.05$ (compared with the controls).
694 [b] Days post-inoculation (dpi).
695 [c] After subjecting seed-only mixtures containing the same concentration of PrP^{Sc} as 1^{st}- or
696 5^{th}-rPrP-fib^{Sc} to a mock QUIC procedure, the same amount of rPrP was added. The
697 solutions were inoculated into mice as controls for rPrP-fibrils.
698 [d] Numbers represent means ± SD.
699 [e] Numbers represent the survival periods of the TSE-positive mice. All non-symptomatic

mice were negative for PrP^{Sc} at 660 dpi.

[f] Numbers represent dpi when the experiment was ended.

[g] A 201-dpi mouse was used.

[h] A 333-dpi mouse was used.

Figure. 1

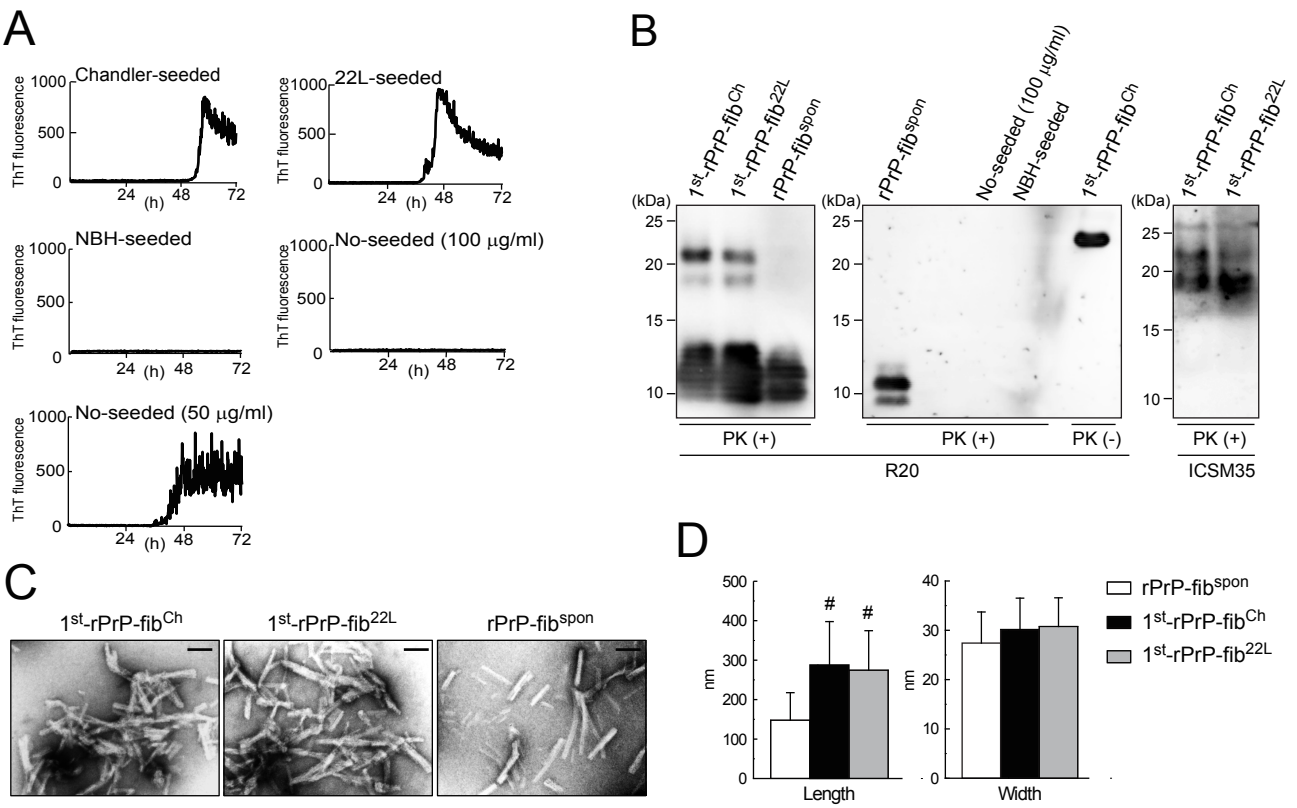
A
Chandler-seeded
22L-seeded
NBH-seeded
No-seeded (100 μg/ml)
No-seeded (50 μg/ml)
ThT fluorescence
1000
500
0
24
48
72
(h)
B
1st-rPrP-fibCh
1st-rPrP-fib22L
rPrP-fibspon
No-seeded (100 μg/ml)
NBH-seeded
(kDa)
25
20
15
10
PK (+)
PK (-)
R20
ICSM35
C
1st-rPrP-fibCh
1st-rPrP-fib22L
rPrP-fibspon
D
rPrP-fibspon
1st-rPrP-fibCh
1st-rPrP-fib22L
nm
Length
Width
#

Figure. 2

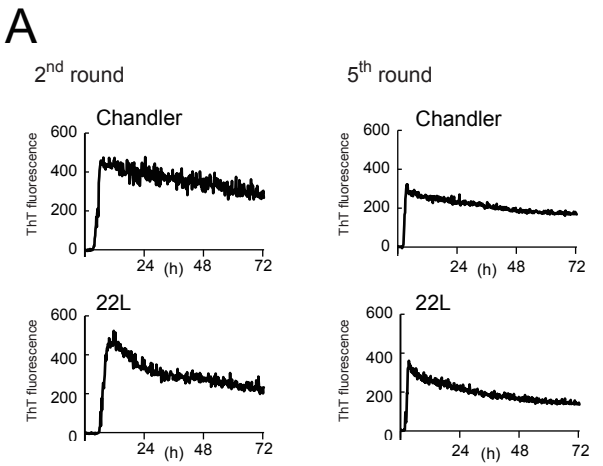
A
2nd round
5th round
Chandler
22L
ThT fluorescence
600
400
200
0
24
(h)
48
72

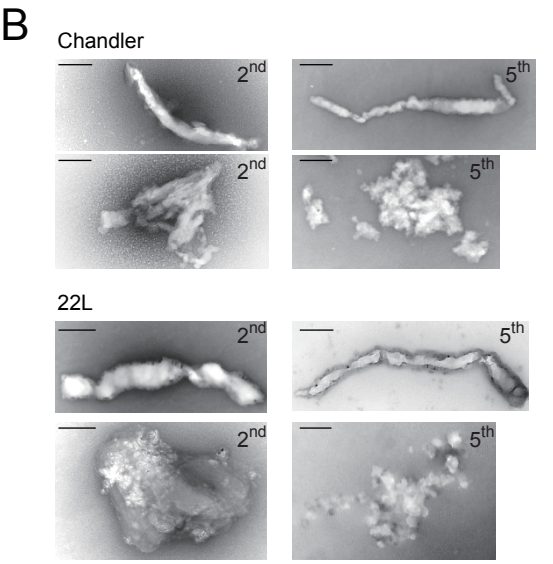
B
Chandler
22L
2nd
5th

Figure. 3

A

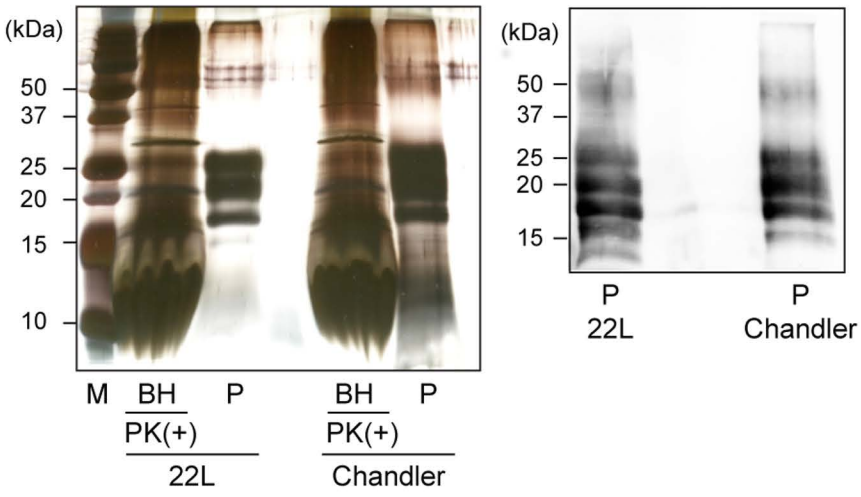
(kDa)
50
37
25
20
15
10
M
BH
P
PK(+)
22L
BH
P
PK(+)
Chandler
(kDa)
50
37
25
20
15
P
22L
P
Chandler

B

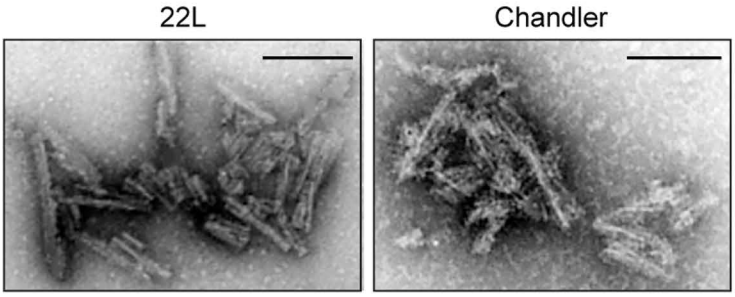
22L
Chandler

Figure. 4

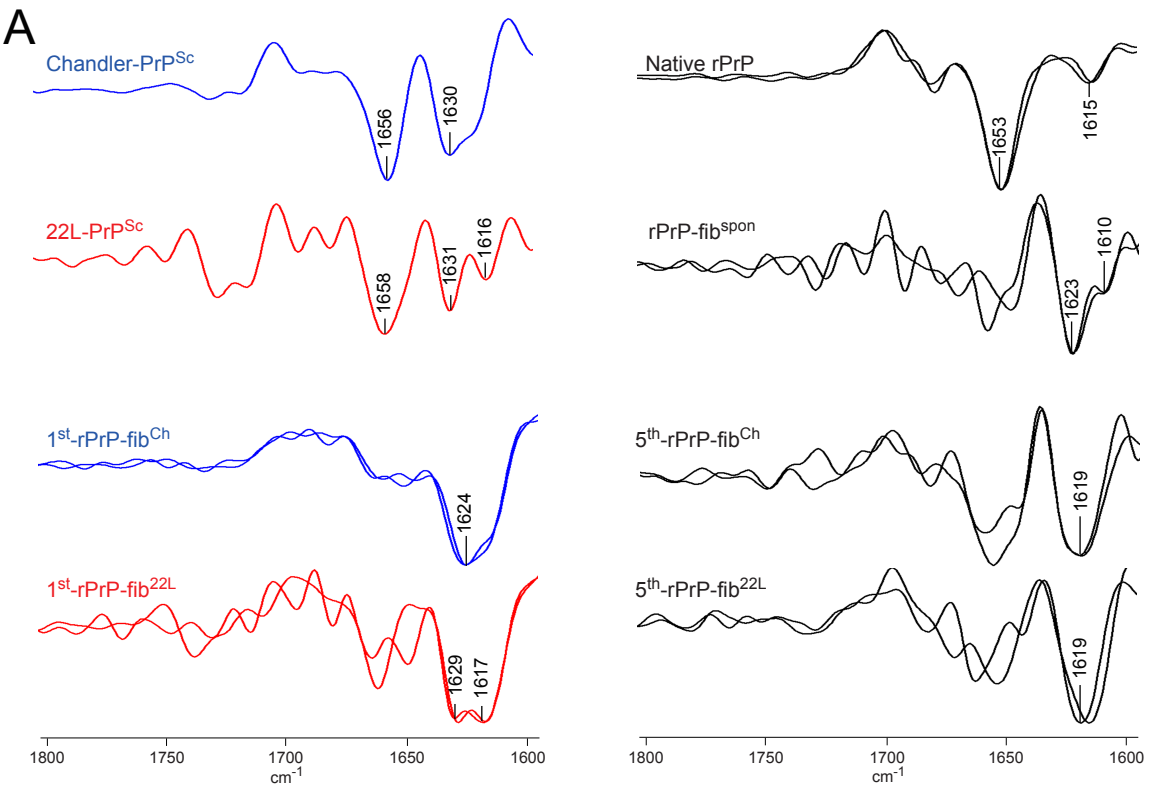
A
Chandler-PrP^Sc
1656
1630
22L-PrP^Sc
1658
1631
1616
1st-rPrP-fib^Ch
1624
1st-rPrP-fib^22L
1629
1617
Native rPrP
1653
1615
rPrP-fib^spon
1623
1610
5th-rPrP-fib^Ch
1619
5th-rPrP-fib^22L
1619
1800
1750
1700
1650
1600
cm-1

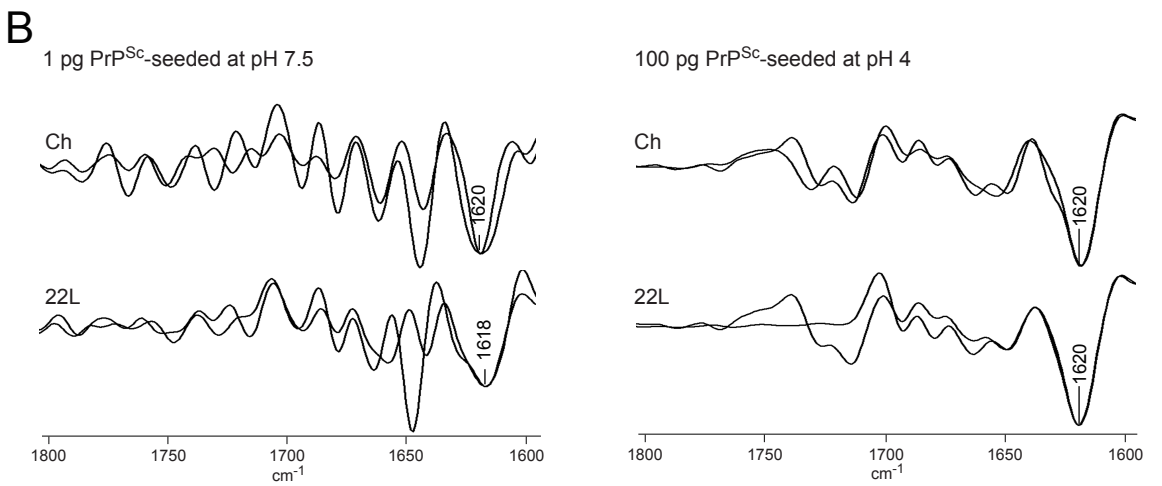
B
1 pg PrP^Sc-seeded at pH 7.5
Ch
1620
22L
1618
100 pg PrP^Sc-seeded at pH 4
Ch
1620
22L
1620
1800
1750
1700
1650
1600
cm-1

Figure. 5

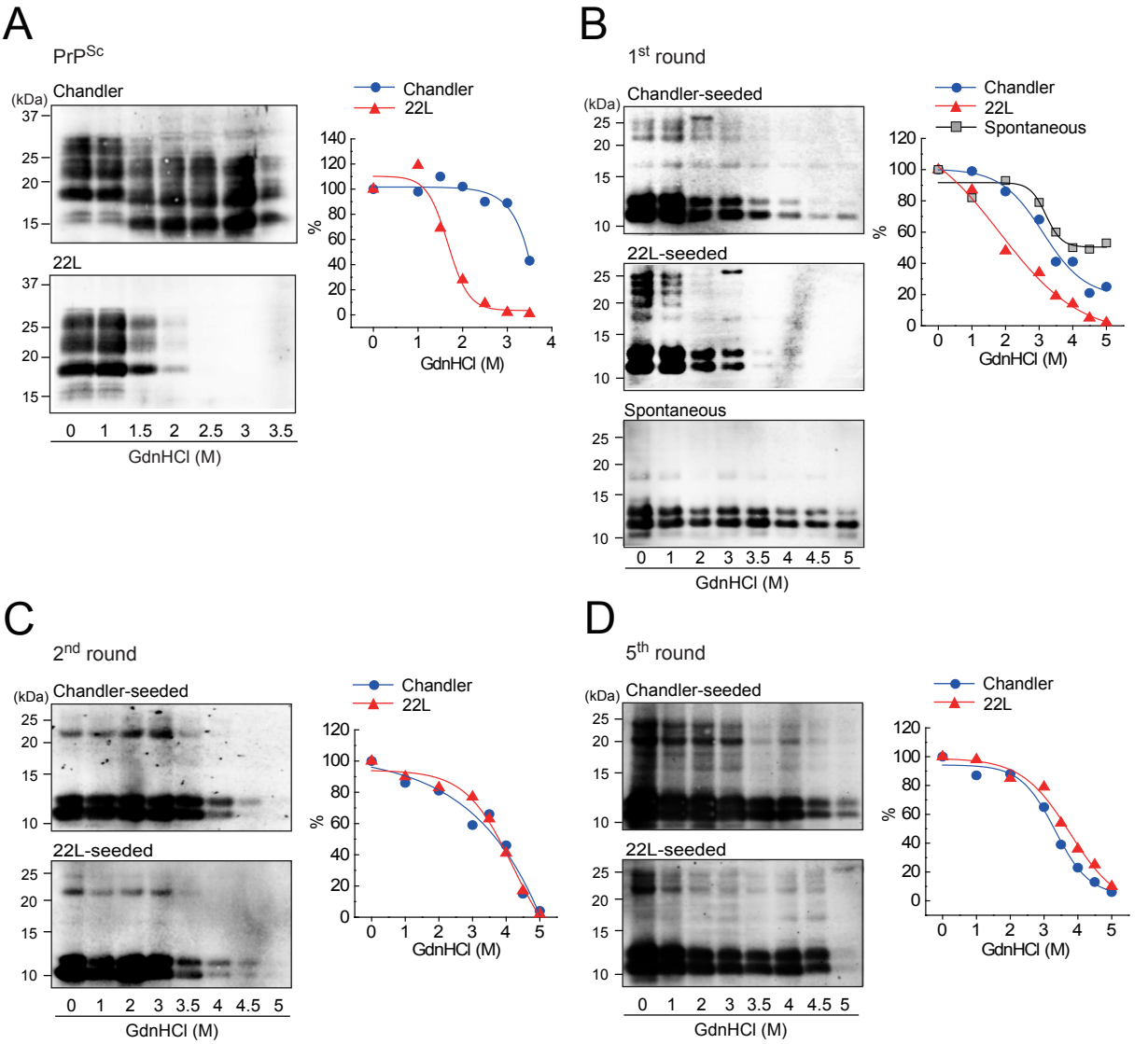
A
PrP^Sc
(kDa)
Chandler
37
25
20
15
22L
0 1 1.5 2 2.5 3 3.5
GdnHCl (M)
Chandler
22L
%
GdnHCl (M)
B
1st round
Chandler-seeded
22L-seeded
Spontaneous
0 1 2 3 3.5 4 4.5 5
GdnHCl (M)
Chandler
22L
Spontaneous
C
2nd round
D
5th round

Figure. 6

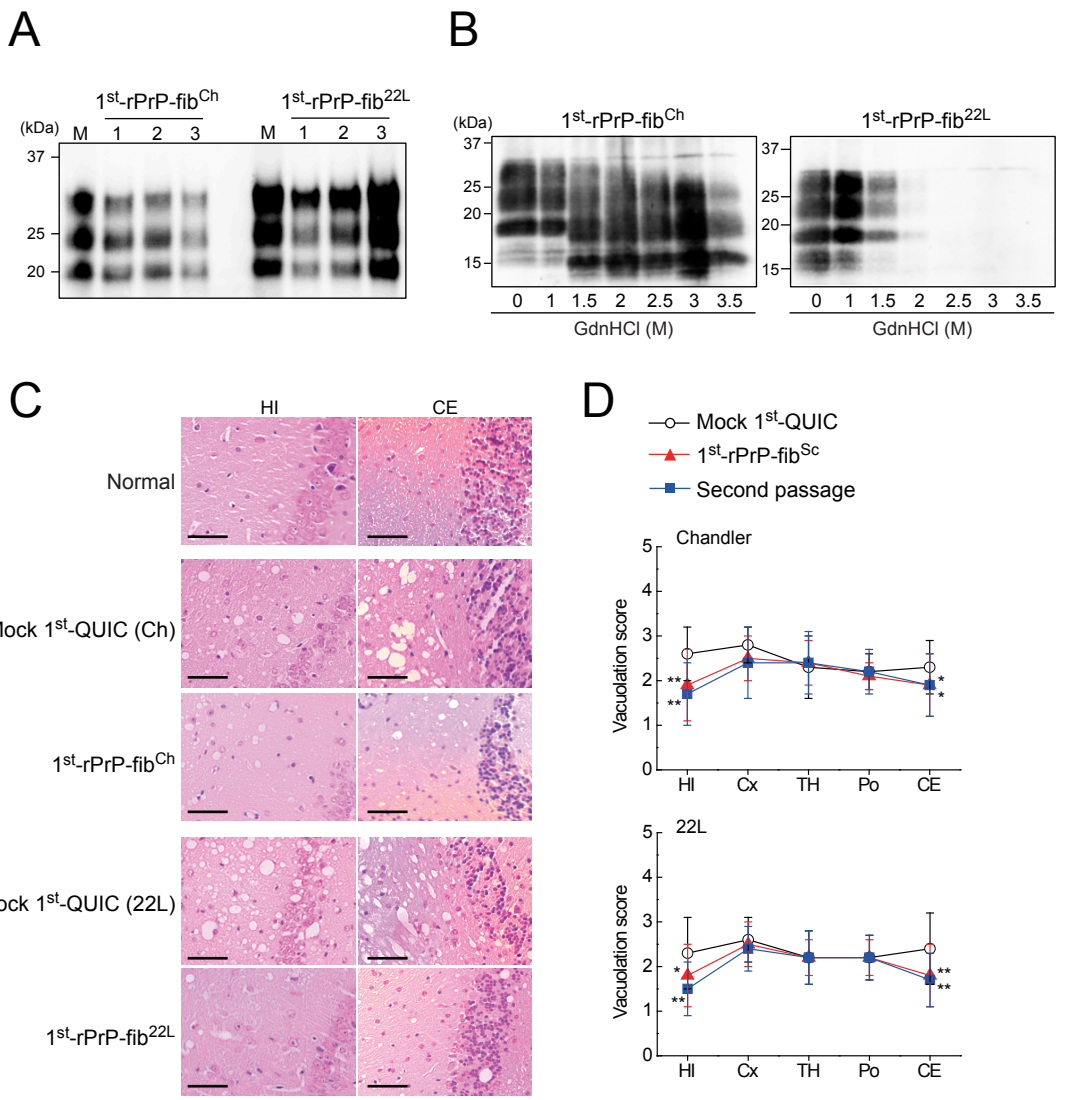
A
1st-rPrP-fibCh
1st-rPrP-fib22L
(kDa)
M 1 2 3 M 1 2 3
37
25
20
B
(kDa)
1st-rPrP-fibCh
1st-rPrP-fib22L
37
25
20
15
0 1 1.5 2 2.5 3 3.5
GdnHCl (M)
C
HI
CE
Normal
Mock 1st-QUIC (Ch)
1st-rPrP-fibCh
Mock 1st-QUIC (22L)
1st-rPrP-fib22L
D
Mock 1st-QUIC
1st-rPrP-fibSc
Second passage
Chandler
Vacuolation score
HI Cx TH Po CE
22L
Vacuolation score
HI Cx TH Po CE